Life Sciences 220 (2019) 136–146

Contents lists available at ScienceDirect

Life Sciences

journal homepage: www.elsevier.com/locate/lifescie

Surface functionalized folate targeted oleuropein nano-liposomes for prostate tumor targeting: *In vitro* and *in vivo* activity

Anmar M. Nassir[a], Ibrahim A.A. Ibrahim[b], Shadab Md[c], Md Waris[d], Tanuja[d], Mohammad Ruhal Ain[e], Iqbal Ahmad[f,*], Naiyer Shahzad[b,**]

[a] Department of Surgery, Faculty of Medicine, Umm Al-Qura University, Makkah, Saudi Arabia
[b] Department of Pharmacology and Toxicology, Faculty of Medicine, Umm Al-Qura University, Makkah, Saudi Arabia
[c] Department of Pharmaceutics, Faculty of Pharmacy, King Abdulaziz University, Jeddah, Saudi Arabia
[d] Department of Botany, Thakur Prasad Singh (TPS) College, Patna, Magadh University, Bodh Gaya, India
[e] Department of Clinical Pharmacy, Prince Sattam bin Abdulaziz University, Alkharj, Saudi Arabia
[f] Formulation Research Lab., Advance Nanomeds, Plot no. 142/20A, NSEZ, Noida 201305, UP, India

ARTICLE INFO

Keywords:
Prostate cancer
Oleuropein
Liposomes
Folate targeting
Long circulation
In vivo anticancer effects

ABSTRACT

Aims: This study aims to develop and evaluate oleuropein loaded surface functionalized folate-targeted – PEG liposomes for the effective management of prostate cancer in an animal model.

Materials and methods: Film hydration-cum-extrusion technique was used to produce liposomes. Particle size, entrapment efficiency, drug loading, electron microscopy, and drug release study were performed for the characterization. Cell viability and various *in vitro* studies (phosphatidylserine internalization, TUNEL assay, measurement of mitochondrial membrane potential and caspase-3 assay) were performed to compare the anticancer and apoptotic effects of developed liposomes against the plain oleuropein. Comparative pharmacokinetic profiling and anticancer efficacy studies including a change in tumor volume, body weight, and survival analysis were performed in mice model.

Key findings: The developed liposomes (OL-FML) showed the particle size of 184.2 ± 9.16 nm, the zeta potential of 1.41 ± 0.24 mV, entrapment efficiency of 63.52 ± 4.15% and drug loading of 21.31 ± 2.37%. OL-FML showed higher *in vitro* anti-proliferative effect and apoptosis on 22Rv1 cells. *In vivo* pharmacokinetic study revealed a nearly 6 fold increase in the bioavailability of OL-FML ($AUC_{0\rightarrow\infty}$ = 641.78 ± 103.764 μg/mL·hr) as compared to OL solution ($AUC_{0\rightarrow\infty}$ = 104.11 ± 18.374 μg/mL·hr) in mice. Increased tumor suppression, weight loss resistance, and survival probability were observed in 22Rv1 induced tumor-bearing mice with OL-FML treatment as compared to OL.

Significance: The study provides conclusive evidence for the utilization of combining passive and active targeting strategy to enhance the anticancer effect of OL.

1. Introduction

According to global cancer statistic 2015, prostate cancer is one of the major cause of cancer death in men. With 1.6 million cases worldwide, it is the fifth leading cause of cancer mortality among men (mortality burden > 300,000 deaths per year) [1]. Furthermore, Castration-resistant prostate cancer (CRPC) is the second leading cause of oncological deaths among the United States men's population (32,000 deaths per year). Treatment of localized tumors are generally curable, however, nearly 25% of the patients develop metastatic castration-resistant prostate cancer which is highly resistant to chemotherapy [2].

Oleuropein (OL), a richly found natural compound in unprocessed olive fruit and leaves is a major constituent of the secoiridoid family. Chemically, it is a heterosidic ester of elenolic acid and dihydroxyphenylethanol, which upon hydrolysis yields other bioactive substances like eleonolic acid and hydroxytyrosol [3]. OL has been shown to possess numerous pharmacological effects which include cardioprotective, antiarrhythmic, hypotensive, spasmolytic as well as anti-inflammatory properties [4]. Moreover, a few *in vivo* and *in vitro* results also suggest its activity against tumor cell growth and invasiveness as

* Corresponding author.
** Correspondence to: Dr. N. Shahzad, Department of Pharmacology and Toxicology, Faculty of Medicine, Umm Al-Qura University, P.O. Box 7607, Holy Makkah 21955, Saudi Arabia.
E-mail addresses: iqbal_ahmad2@yahoo.co.in (I. Ahmad), shahzadnaiyer@gmail.com (N. Shahzad).

https://doi.org/10.1016/j.lfs.2019.01.053
Received 20 September 2018; Received in revised form 26 January 2019; Accepted 29 January 2019
Available online 31 January 2019
0024-3205/

well as angiogenesis [5–7]. OL has also been shown to possess some activity against prostate cancer cell lines. Acquaviva et al. studied the effects of OL on prostate cancer cell lines, LNCaP, and DU145 in comparison to non-malignant BPH-1 cells. They concluded that OL lessens the cell viability through pro-oxidant mechanisms on cancer cells while it shows antioxidant effects on BPH-1 cells [6]. Although, with a wide range of established bioactivities in the laboratory, this molecule is still far from being included into mainstream therapeutics. Oral pharmacokinetic profile of OL being one of the major setbacks. Boccio et al. showed that after oral administration of a 100 mg/kg of OL in rats, C_{max} of only 200 ng/mL was detected in plasma at 2 h [8]. Another study conducted on freely moving rats showed that only 0.5% of OL is bioavailable when given orally [9]. Moreover, a human pharmacokinetic study concludes that there is a rapid absorption, metabolism and renal clearance of olive phenolic compounds (OL and HT) after oral administration. Also, the bioavailability and metabolism of oleuropein were found to be highly heterogeneous and dependent on formulation characteristics as well as gender [10]. So, to overcome the drawback of oral administration, the intravenous route is generally preferred. However, there is no study that clearly demonstrates the pharmacokinetic profile of OL after i.v. administration in animal models. Moreover, due to rapid metabolism and clearance, minimal exposure to the prostate tissue is expected. So, for effective use of OL in prostate cancer management, there is a need of a long-circulating intravenous system that could avoid the hindrances caused by oral route and would be effectively targeting the prostate cancer cells.

Liposomal drug delivery systems have been extensively explored for the delivery of anticancer drugs during the last two decades because of its ability to encapsulate both hydrophilic and hydrophobic drugs, biocompatibility, passive/active target-ability as well as the possibility of their expedited cellular uptake and cytoplasmic delivery [11]. In relation to the application of liposomes in prostate cancers, most of the preclinical studies have utilized the passive targeting of anticancer drugs through EPR (enhanced permeation and retention) effect, thereby achieving greater efficacy, lowering the total effective dose and consequently decreasing the side effects [12]. PEGylated or stealth liposomes show additional benefits of longer circulation through RES (reticuloendothelial system) escape mechanism. The combined effect of RES escape and EPR enhances the targeting efficiency of liposomes in Non-RES organs [13]. Many studies have also focussed on active (ligand-mediated) liposomal targeting of tumor cells. Different targeting strategy and surface functionalization techniques of liposomes and its use in solid tumors have been extensively reviewed [14]. An active targeting strategy utilizing liposomes for prostate targeting was developed by Xiang et al. They dually incorporated prostate-specific antigen (PSA) responsive activatable cell-penetrating peptide moiety and prostate-specific membrane antigen (PSMA) targeted folate moiety into siRNA loaded liposomes. They showed that folate moiety actively bonded to PSMA-positive tumors, while PSA-responsive moiety was cleaved by PSA to expose cell-penetrating peptide. The dually activated liposomes (folate and cell-penetrating peptides) were internalized by tumor cells. They concluded that targeting capacity and therapeutic potency of the developed system presented a promising strategy for prostate cancer theranostics [15]. From the published findings, it can be concluded that the effect of oleuropein on prostate cancer cells has been established and few reports show the incorporation of oleuropein into nanocarriers. However, till now none have compared the effect of plain oleuropein with oleuropein loaded nanocarrier system in the *in vitro* and *in vivo* prostate cancer model. Thus, in this study we exhibit the development and characterization of folate decorated oleuropein liposomes; establish pharmacokinetics of OL and OL loaded folate decorated PEG-liposomes through intravenous route, compare the effectiveness of the prepared system in human prostate cancer cell line with plain oleuropein; and evaluate *in vivo* anticancer activity of the prepared system in tumor-bearing mice with respect to plain oleuropein.

2. Materials and methods

2.1. Materials

Oleuropein (98%) was obtained from Sigma Aldrich Sigma Aldrich Co. (St. Louis, MO, USA). 1,2-distearoyl-sn-glycero-3-phosphoethanolamine-*N*-[folate(polyethylene glycol)-5000] (ammonium salt) (DSPE-PEG(5000)) and 3β-[*N*-(*N′*,*N′*-dimethylaminoethane)-carbamoyl] cholesterol hydrochloride (Cholesterol DC) was procured from Avanti Polar Lipids Inc., Alabaster, AL, USA. All other chemicals and reagents were of analytical grade and used without further purification.

2.2. High-performance liquid chromatography (HPLC)

The RP-HPLC method presented by Grizis et al., modified and used to quantify OL in both formulation and plasma [16]. A binary pump enabled UV–Visible based HPLC system with a manual injector system (HPLC-3000, Analytical Technologies Ltd., India) was used to cross-validate the method. The data analyses of the method were performed through CXTH-3000 software. ACE® 5 C18 column (250 mm × 4.6 mm, 5 μm) (Advanced Chromatography Technologies Ltd., Scotland) was used for separation. Methanol: acetic acid 2% aqueous solution (45: 55 v/v) was used as mobile phase with a flow rate of 1 mL/min). Injection volume was 20 μL and a detection wavelength was set at 279 nm. Six dilutions of OL with concentrations ranging from 10 to 200 μg/mL were prepared in Methanol: 0.1 M phosphate buffer saline, pH 7.4 (PBS) (99:1 v/v) solution for the calibration curve.

For the calibration curve in plasma, standards were prepared by spiking 90 μL aliquots of pooled drug-free plasma with 10 μL of methanolic dilutions of OL to make final concentrations ranging from 0.1 to 2.0 μg/mL.

For extraction of OL, 50 μL of 0.5 M HCl was added to 100 μL of plasma sample and vortexed for 15 s. 10 mg of anhydrous sodium sulfate was then added and dissolved by vortex. 300 μL of ethyl acetate was consequently added to each sample, vortexed for 2 min and centrifuged for 5 min at 2000 rpm. The supernatant organic layer was transferred into a 1 mL centrifuge tube. The leftover aqueous layer was again extracted with 300 μL of ethyl acetate. The combined ethyl acetate layer was evaporated at 50 °C under a gentle stream of nitrogen. The dry residue was reconstituted in 100 μL of mobile phase and 20 μL sample was injected into the HPLC system.

2.3. Preparation of oleuropein-loaded liposome

Oleuropein loaded folate-modified liposomes (OL-FML) were prepared by the method described by Xiang et al. with some modifications [15]. Briefly, a 100 mg mixture of SPC (48%), DC-cholesterol (40%), Cholesterol (8%), DSPE-mPEG2000 (3%) and DSPE-PEG5000-Folate (1%) were taken in a 500 mL round bottom flask and dissolved in chloroform: methanol (3:1 v/v). Using a rotary evaporator, the solvent was removed under vacuum to form a thin lipid film. 5 mL of 20 mg/mL aqueous solution of OL was added to the lipid film and rotated using rotary evaporator under a nitrogen atmosphere for 6 h at 50 °C. The lipid dispersion was then sequentially extruded 10 times through 400 nm and 200 nm polycarbonate membranes using a manual extruder (Avanti, Canada) to control liposomal size. The liposomal dispersion was then centrifuged at 12,000 rpm for 1 h. The pellet was washed twice with 0.1 M phosphate buffer saline, pH 7.4 (PBS) and re-dispersed in the same medium by vortexing. The dispersion was lyophilized for storage and reconstituted in PBS whenever required.

2.4. Formulation characterization

2.4.1. Visual observation

10 mg of the OL-FML was dispersed in 50 mL PBS with vigorous

shaking and visually observed under white light for a characteristic opalescence and presence of any particle aggregates.

2.4.2. Particle size distribution and zeta potential

Vesicular size of the OL-FML was measured by using Zetasizer (Nano-ZS, Malvern Instruments, UK). Here, 10 mg of the lyophilized formulation was diluted in 100 mL of PBS with vigorous shaking. 0.5 mL of the sample was taken in a disposable zeta sizing cuvette and analyzed at 25 °C at a measurement angle of 90°. Zeta potential was also determined using the same instrument employing zeta potential cuvette.

2.4.3. Scanning electron microscopy

Surface morphology of freeze-dried liposomes was observed under a scanning electron microscope. The dried samples were coated with 5 nm gold and photomicrographs were obtained from a Zeiss Gemini 5 1530 FEG scanning electron microscope (Carl Zeiss Microscopy GmbH, Jena, Germany).

2.4.4. Transmission electron microscopy

Morphology of the liposomes was observed by transmission electron microscopy. A transmission electron microscope (JEOL 2100F) capable of a 0.18 nm point to point resolution was set at 200 kV. The dispersed liposomal sample was directly deposited on the holey film grid and observed after drying.

2.4.5. Entrapment efficiency and drug loading

100 mg of the lyophilized formulation was dispersed in 10 mL of PBS and 0.1%w/v of Triton X-100 added and vortexed for the lysis of liposomes. The lipid dispersion was then subjected to ultracentrifugation at 12000 rpm for 1 h. 100 μL of the supernatant was diluted with 9.9 mL of mobile phase (dilution factor = 100) and analyzed by HPLC method described in earlier section. The entrapment efficiency (%EE) and drug loading (%DL) was calculated by the following formula:

$$\%EE = [\text{OL found in the liposomes/amount of OL added}] \times 100\%DL$$
$$= [\text{OL found in the liposomes/Total weight of liposomes}] \times 100$$

2.4.6. Differential scanning calorimetry (DSC)

Differential scanning calorimeter (Perkien Elmer, USA) was used to study the thermal behavior of liposomes and plain OL. 10 mg each of lyophilized liposome samples and equivalent amount of plain OL was put in hermetic aluminium pans and heated under an inert nitrogen atmosphere at a rate of 10 °C/min over the range of 20–200 °C. Empty aluminium pans were used as reference.

2.4.7. In-vitro drug release

The drug release from OL loaded liposome was performed using the dialysis bag method. The dialysis bags (MWCO 12KD, Sigma) were activated using the standard procedure. 1 mL of re-constituted liposomes (containing 100 mg/mL of OL, calculated on the basis of %DL) was put into the dialysis bag and placed in a beaker containing 100 mL dissolution medium kept at 37 °C, pre-stirred at 100 rpm. An aliquot of the dissolution medium (0.1 mL) was withdrawn at time intervals of 0.25, 0.5, 0.75, 1, 2, 3, 4, 5, 6, 8, 12, 18, 24 h. The sample (0.1 mL) was mixed with 9.9 mL of methanol and analyzed by the HPLC method described previously.

2.5. In vitro activities on 22Rv1 cells

2.5.1. Cell culture

The human prostate cancer cell line 22Rv1 (ATCC® CRL-2505™) was procured from ATCC and grown in RPMI 1640 medium at 37 °C (pH 7.4) supplemented with 10% fetal bovine serum (FBS), penicillin (100 IU mL^{-1}) and streptomycin (100 μg mL^{-1}) and 2 mM L-glutamine in a humidified atmosphere of 5% CO_2. The cells were sub-cultured in fresh RPMI-1640 medium at an average density of 2×10^5 cells mL^{-1}.

2.5.2. Cell viability study by MTT assay

MTT [3-(4,5-dimethylthiazol-2-yl)-2,5-diphenyltetrazolium bromide] assay was performed as per the method reported previously [17]. In a flat bottom 96-well plate, 5×10^4 counts (200 μL) of cells were seeded and incubated in 5% CO_2 at 37 °C for 48 h. Plain OL aqueous solution and aqueous OL-FML dispersion were added to the wells OL concentrations of 50, 100 and 250 and 500 μM. 2 mL of MTT solution (5 mg/mL) was added to each well and incubated (37 °C/5% CO_2). After 4 h of incubation, the medium of each well was replaced with 2 mL of DMSO and the optical density was measured at 570 nm. Percentage cell viability was calculated as a measure of the optical density ratio of treated and untreated sample.

2.5.3. Cell apoptosis studies

2.5.3.1. Phosphatidylserine externalization assay. As previously reported, we evaluated the phosphatidylserine (PS) externalization as a measure of cell apoptosis. Double staining technique with Annexin-V and PI was utilized for PS externalization assay. OL and OL-FML in the concentrations of 50, 100, 250 and 500 μM were administered to 22Rv1 cells and incubated for 24 h at 37 °C under 5% CO_2 humidified condition. Consequently, the cells were centrifuged (10 min, 3000 × *g*), washed twice in cold PBS, re-suspended in 100 μL Annexin V-FLUOS labeling solution and incubated (15 min, dark, 26 °C). After which, 400 μL of incubation buffer was added, mixed and observed under flow cytometer (BD LSR II) [18].

2.5.3.2. TUNEL assay. TdT (Terminal deoxynucleotidyl transferase) mediated Nick end labeling method was used to study DNA fragmentation. OL and OL-FML in the concentrations of 50, 100, 250 and 500 μM were administered to 22Rv1 cells. The cells washed with PBS and 4% paraformaldehyde was added for fixation and incubated on ice for 1 h. Cells were again washed and 3% H_2O_2 in methanol was added and incubated for 10 min at 25 °C. After washing the cells with PBS, freshly prepared chilled Triton X-100 solution (0.1%v/v) was added for cell membrane perforation. Now, cells were washed and incubated (37 °C for 1 h) after addition of 50 mL of reaction mixture containing FLUOS-labelled dUTP and TdT. The cells were washed, re-suspended in PBS, and observed under a flow cytometer [18]. Untreated cells were observed as a control.

2.5.3.3. Measurement of mitochondrial membrane potential (Δψm). Mitochondrial membrane potential (Δψm) was determined by analysis of JC-1 dye retention in 22Rv1 cells [17]. 1 μg/mL of JC1 dye was loaded in OL, OL-FML treated or untreated cells (5×10^4 per well), incubated (30 min, 37 °C, 5% CO_2) and washed twice with PBS. J-aggregate of JC1 was analyzed by fluorescence measurement at 570 nm excitation/595 nm emission. Mitochondrial membrane potential was measured as the ratio of the fluorescence intensity of J-aggregate (aqueous phase) and monomer (membrane-bound) forms of JC1.

2.5.3.4. Caspase-3 assay. 5×10^4 per well of the 22Rv1 cells were seeded in 96-well plate containing 200 μL culture medium. After 16 h, equivalent doses of 50, 100, 250 and 500 μM of OL solution and OL-FML were put into the wells to induce apoptosis. Caspase-3 activity was observed as per the method prescribed in Caspase-3 kit manual (EMD Biosciences) and analyzed using a fluorometer [19].

2.5.4. In-vivo studies

2.5.4.1. Animals. 6-week-old male BALB/c nude mice (30 ± 2 g) were used for all the in vivo studies. Proper authorization was obtained from Committee of Bio-Medical Ethics, Umm Al-Qura University, Holy Makkah, KSA, and their guidelines were adhered to for the complete duration of the study (Approval no. HAPO-02-K-012-2016-05-160). The

animals were kept under standard laboratory conditions i.e. 25 ± 2 °C, 55 ± 5% RH, housed in polypropylene cages, with free access to standard laboratory diet and water ad libitum.

2.5.4.2. In vivo pharmacokinetic studies. 12 BALB/c male nude mice (30 ± 2 g) were divided into 2 groups ($n = 6$). The aqueous dispersion of OL and OL-FML (containing OL concentration of 5 mg/mL) were prepared in phosphate buffer saline (pH 7.4) and sterilized as per the method described by [20]. 150 μL of the sterilized OL and OL-FML (dose equivalent = 25 mg/Kg) was administered to the group I and group II respectively through the tail vein. 30 μL of blood was withdrawn from the saphenous vein at the time point of 0.5, 1, 2, 8, 16, 24 and 48 h. The blood samples were kept in heparinized tubes and plasma was obtained by centrifugation. OL was extracted from plasma by liquid-liquid extraction and analyzed by HPLC method.

2.5.4.3. Biodistribution study. 22Rv1 cells (1.0×10^6 cells) were subcutaneously injected in 54 BALB/c male nude mice for the induction of tumor growth. After 12 days (tumor size ~0.1 cm^3), they were divided into three groups with 18 mice in each. 150 μL of the sterilized OL (plain solution), OL-L (liposomes without targeting moiety), OL-FML (liposomes with targeting moiety) (dose equivalent = 25 mg/Kg) were intravenously administered to group I, II and III respectively. At each time points of 0.5, 2, 8, 16, 24 and 48 h with respect to respective injection time (time zero), 3 animals were anesthetized and dissected to extract different organs (liver, spleen, kidney, heart and lungs) as well as whole tumor volume. They were blotted dry using paper tissue, weighed and 2 mL/g tissue mass of ice-cold KCl solution was added. The mixture was homogenized in a tissue homogenizer and centrifuged (4000 rpm, 4 °C, and 15 min). The supernatant was extracted for OL as per the method described for plasma in HPLC section and analyzed.

2.5.4.4. Induction of tumor in nude mice and dosing regime. Antitumor efficacy of the developed OL-FML was compared with OL solution in a xenograft tumor model. 22Rv1 cells (1.0×10^6 cells) were subcutaneously injected in BALB/c male nude mice. After 12 days, tumor size of approximately 0.1 cm^3 was observed. The mice were then randomly divided into three groups ($n = 10$). To the groups I, II and III the mice were intravenously administered normal saline (Tumor Control), plain OL solution (25 mg/kg), and OL-FML dispersion in NS (containing OL dose equivalent to 25 mg/Kg) respectively. The doses were administered every 24 h for 30 days. Group IV mice (Normal Control; $n = 10$) were not induced with the tumor but the normal saline was administered at each dosing time.

2.5.4.5. Change in tumor volume. Tumor volume (TMV) for each passing day was recorded and represented on TMV vs time curve. The tumor volume was calculated using the formula.

$$TMV = (length \times width^2)/2$$

2.5.4.6. Change in body weight. Average body weights of each group were recorded daily for 30 days and percentage change in body weight vs time graph was plotted.

2.5.4.7. Kaplan–Meier survival analysis. Survival probability for 30 days was calculated as a number of animals surviving at the start of each day divided by the number of animals at risk. Each term in the product is the *conditional probability* of survival beyond time t_i, given the subject has survived up to time t. Cumulative survival probability, s(t) was obtained by the following equation:

$$s(t) = \prod_{ti \le t} \frac{n_i - d_i}{n_i}$$

where, n_i = number of animals at the starting of the day, and d_i = number of death.

2.6. Statistical analysis

All the quantitative data were expressed as an average ± SD. In all cases, comparisons between two groups of observations were made using the 2-tailed Student's *t*-test. However, for *in vitro* activities, significance level at each concentration was compared between OL and OL-FML treatments. Log-rank test was used to analyze Kaplan-Meier survival curve. Values of $p < 0.05$ were considered to be statistically significant.

3. Results

3.1. Formulation characterization

3.1.1. Visual observation

The dispersion of OL-FML in PBS was found to be transparent with a characteristic opalescence. Also, there was no suspended particulate matter visible.

3.1.2. Particle size distribution, zeta potential

OL-FML showed a particle size of 184.2 ± 9.16 nm (Fig. 1A). Also, the poly dispersity index (PDI) revealed a fairly uniform particle size distribution (PDI = 0.113 ± 0.088). Zeta potential of OL-FML was found to be 1.41 ± 0.24 mV (Fig. 1B).

3.1.3. Entrapment efficiency (%EE) and drug loading

The percentage entrapment efficiency and drug loading of the formulation were determined to be 63.52 ± 4.15% and 21.31 ± 2.37% respectively.

3.1.4. Scanning and transmission electron microscopy

Transmission electron microscopic (TEM) images revealed distinct spherical boundaries of the liposomes with a narrow particle size distribution. TEM photomicrograph of the selected formulation is given in Fig. 2A. Furthermore, the representative scanning electron micro-photograph of the freeze-dried liposome is shown in Fig. 2B. The image shows aggregates of liposomes having non-smooth surface.

3.1.5. Differential scanning calorimetry

DSC analysis revealed the melting point of OL to be 88.12 °C (Fig. 3A). The lyophilized formulation, OL-FML showed multiple peaks with varying intensity. There were no OL peaks observed in OL-FML DSC curve (Fig. 3B).

3.1.6. In-vitro drug release

The in-vitro release profiles of OL-FML in PBS pH 7.4 showed a controlled release behavior with a maximum release of 78.12 ± 3.88% in 24 h. OL solution released > 75% of OL from the dialysis membrane within 1 h (Fig. 4).

3.2. In vitro activities on 22Rv1 cells

3.2.1. Cell viability study by MTT assay

MTT assay revealed both OL solution ($p < 0.05$) and OL-FML ($p < 0.01$) showed the cytotoxic effect on 22Rv1 cells when compared with normal control (98.6 ± 0.92% cell viability). However, inhibition of cell viability was significantly higher with OL-FML as compared to OL solution at all concentrations (50–500 μM) ($p < 0.05$). Both the treatments showed a dose-dependent increase in 22Rv1 cell viability. For the calculation of IC_{50}, all non-zero concentrations were converted to log values and the plot was transformed to Log concentration [μM] vs % Cell viability. The IC_{50} was calculated as the antilog of Log concentration that kills 50% of the cells. IC_{50} was found to be 391.47 ± 1.22 μM and 132.23 ± 1.12 μM respectively for OL solution

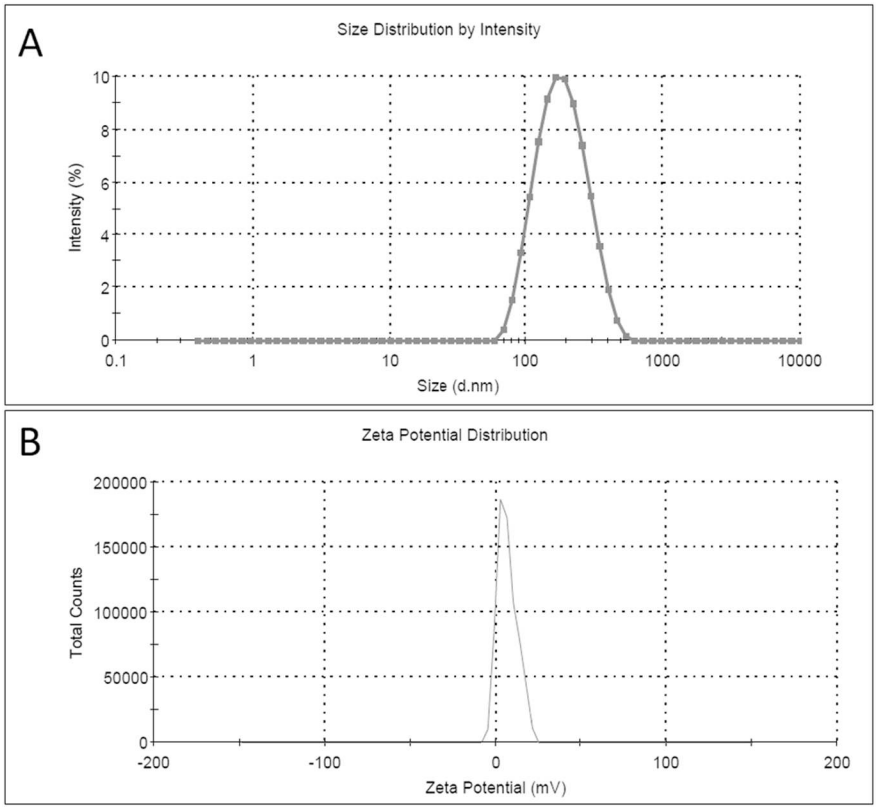

Fig. 1. A) Particle size and B) zeta potential distribution of the developed liposome (OL-FML).

and OL-FML (Fig. 5).

3.2.2. Cell apoptosis studies

3.2.2.1. Phosphatidylserine externalization assay. Annexin V/PI dual staining technique was used to differentiate between the stages of apoptosis. In the early stage of apoptosis, phospholipids translocate towards the outer layer of the plasma membrane. Annexin V has a high affinity for phosphatidylserine (PS) and thus used to show PS externalization. However, annexin V can also label necrotic cells. So, propidium iodide (PI) is used additionally to differentiate between live cells (annexin V- and PI-), the early apoptotic cells (annexin V + and PI-), late apoptotic cells (annexin V + and PI +) and necrotic cells (annexin V- and PI +). In our study, Percentage Annexin V binding was significantly higher with both OL and OL-FML as compared to control (6.55 ± 0.95%) at all concentrations. A maximum of 77.36 ± 3.67%

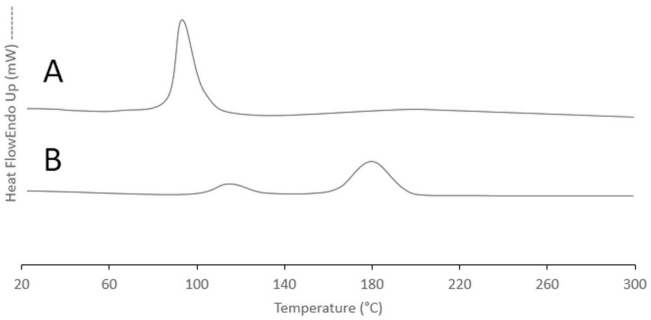

Fig. 3. Differential scanning calorimetric thermogram of A) Oleuropein and B) OL-FML.

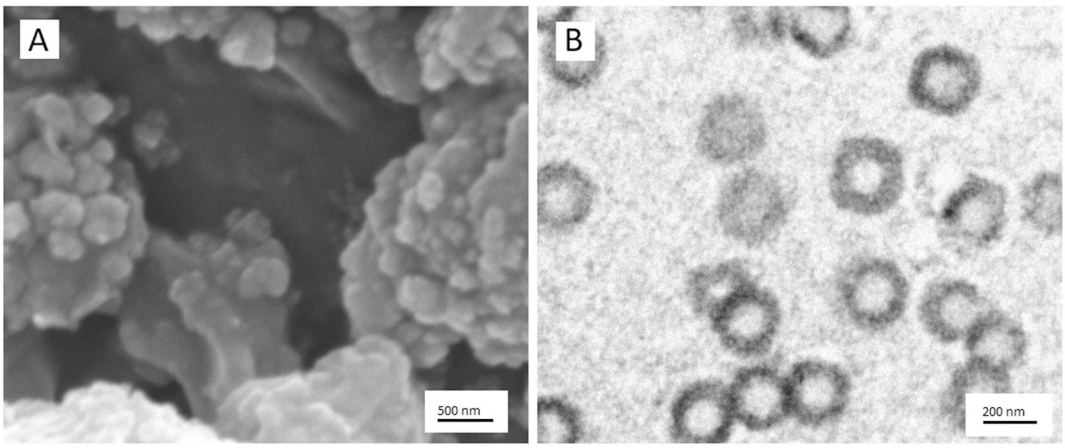

Fig. 2. A) Scanning and B) Transmission electron microscopic images of OL-FML.

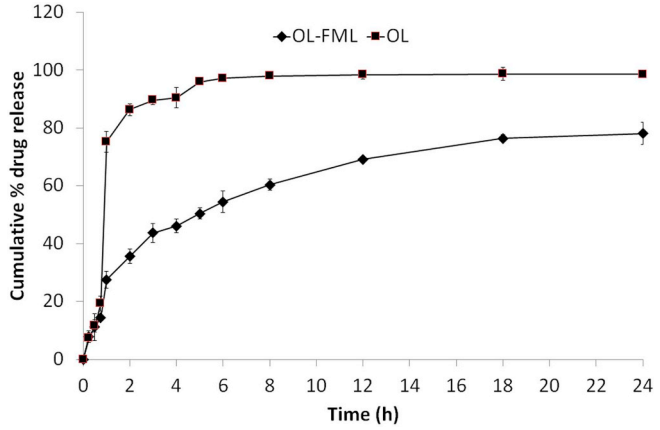

Fig. 4. The comparative drug release profile of OL and OL-FML.

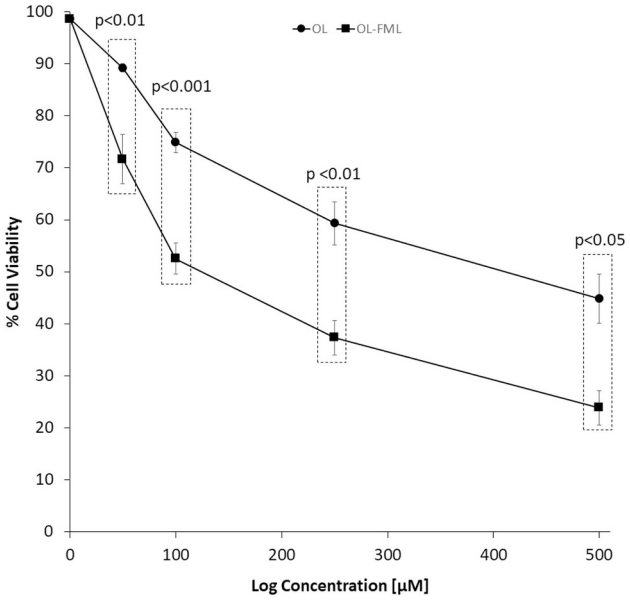

Fig. 5. % Cell viability vs concentration chart for the determination of IC_{50} after OL and OL-FML treatment of 22Rv1 cells.

and 27.9 ± 1.63% of Annexin V binding was observed at 500 µL with OL-FML and OL solution respectively (Fig. 6).

3.2.2.2. TUNEL assay. During apoptosis, the nuclear DNA breaks into nucleosomal units, which expose some DNA nicks. dUTP– FLUOS binds to these nicked ends through TdT. Thus, the fluorescence intensity obtained from dUTP–FLUOS provides a measure of the magnitude of fragmentation. Significantly higher DNA nicking was observed in 22Rv1 cells when treated with OL and OL-FML in a dose-dependent manner as compared to control. There was a remarkable increase in the mean fluorescence intensity (MFI) with OL-FML treatment as compared to OL solution at each dose in varying significance levels. MFI obtained with OL and OL-FML at all the treatment concentrations are presented in Fig. 7.

3.2.2.3. Measurement of mitochondrial membrane potential ($\Delta\psi m$). Fluorescent cationic dye, JC-1 freely permeates to the mitochondrial membranes of the viable cells to form red J-aggregates and emits red fluorescence. Due to reduction mitochondrial membrane potential in apoptotic cells, JC-1 remains as cytosolic monomers and emits green fluorescence. The ratio of J-aggregates (red) to monomers (green) is thus a measure of mitochondrial membrane potential which

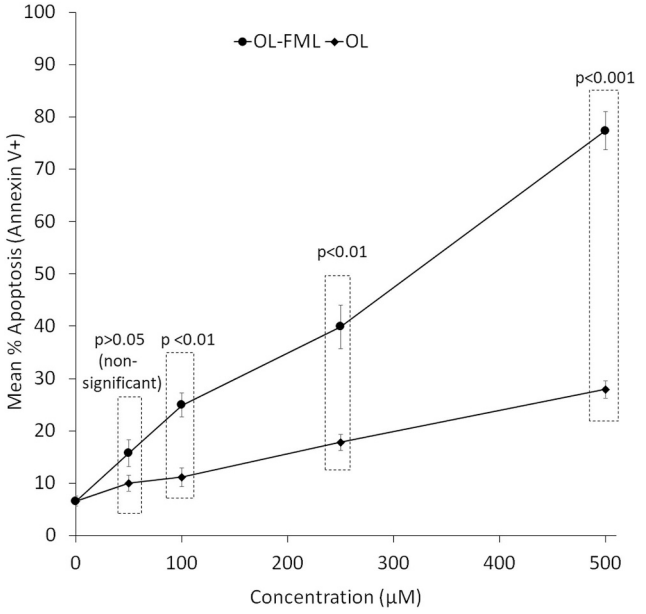

Fig. 6. Mean % apoptosis study by phosphatidylserine externalization assay method.

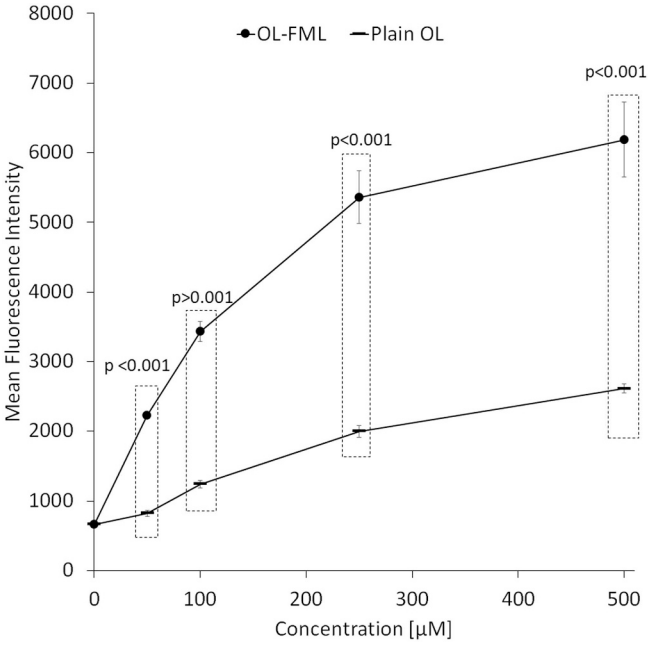

Fig. 7. Comparative TUNEL assay. Mean fluorescence intensity was determined as a measure of the amount of DNA nicking.

is indicative of apoptosis. In control 22Rv1 cells, the red/green fluorescence ratio was found to be 17.9 ± 1.51. The respective decline with the treatment of varying concentration of OL and OL-FML was observed. However, the effect was significantly pronounced with OL-FML as compared to OL ($p < 0.05$) (Fig. 8).

3.2.2.4. Caspase-3 assay. Caspase-3 acts through aspartate-specific cleavage of numerous cellular substrates and its increase is a general marker for the detection of both apoptosis and inflammation. Treatment with OL and OL-FML showed varying degree of increase in caspase-3 activity in a dose-dependent manner. Liposomal formulation caused a significantly higher increase in caspase-3 activity as compared to OL-FML (Fig. 9).

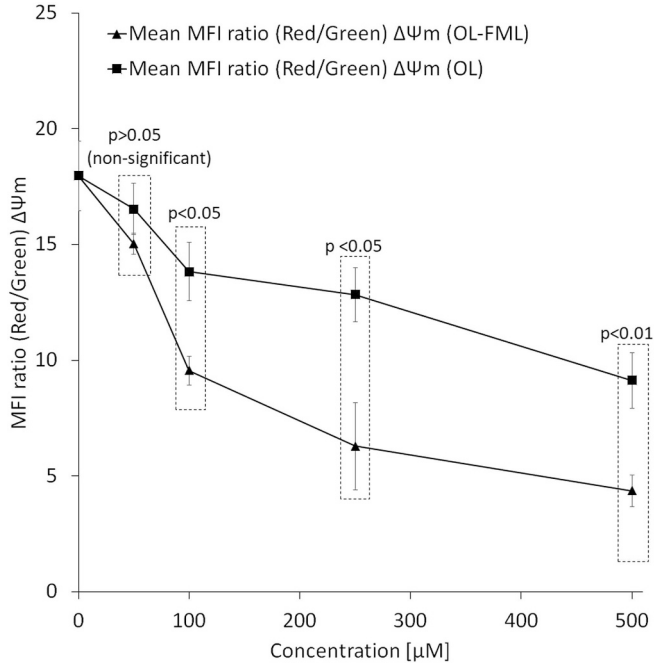

Fig. 8. Mitochondrial membrane potential determination after OL and OL-FML treatment of 22Rv1 cells at various concentrations.

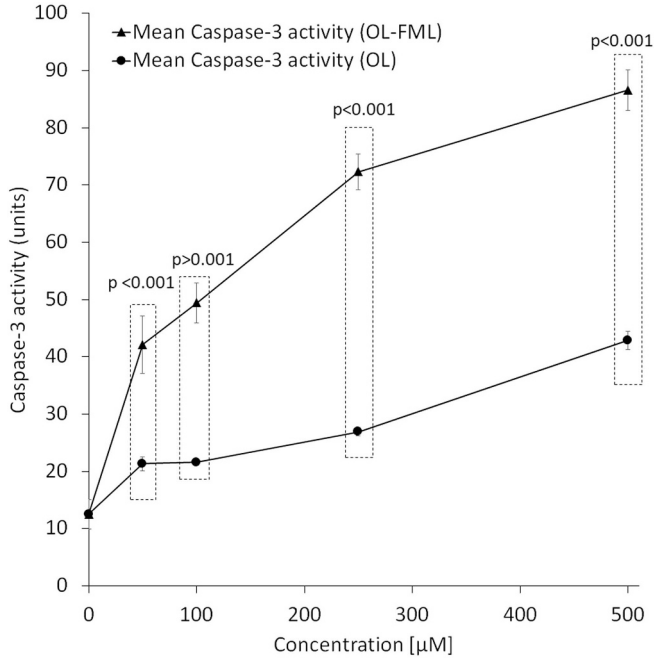

Fig. 9. Caspase-3 activation profile.

3.3. In-vivo studies

3.3.1. In vivo pharmacokinetic and biodistribution study

The comparative intravenous pharmacokinetic profile of OL-FML and OL solution suspension and has been presented in Fig. 10A. The data revealed that there was > 6 times increase in AUC with OL-FML ($AUC_{0-\infty}$ = 641.78 ± 103.764 μg/mL·hr) as compared to OL-Solution (104.11 ± 18.374 μg/mL·hr). Different pharmacokinetic parameters were calculated and have been listed in Table 1. The results of biodistribution study are shown in Fig. 10B. The concentration vs time plots in different organs (Heart, Liver, Lungs, Kidney and Spleen) as well as excised tumor are presented. The tumor targeting effect was well pronounced with OL-FML as compared to OL and OL-L. There was a sustained concentration of OL at the tumor site with 0.83 ± 0.034 μg/g even after 48 h of i.v. administration. With OL-L, there was a gradual increase in concentration upto a maximum of 0.61 ± 0.073 μg/g in 8 h.

3.3.2. Change in tumor volume

Tumor volume was measured each day for 30 days and it was observed that tumor control (group I) had the highest rate of tumor growth with a maximum of 442 ± 12.832% on the 30th day (From 0.11 ± 0.011 cm^3 to 0.56 ± 0.050 cm^3). The rate of tumor increase was significantly lower in both OL ($p < 0.05$) (From 0.11 ± 0.002 cm^3 to 0.40 ± 0.039 cm^3) and OL-FML treatment ($p < 0.01$) groups (From 0.12 ± 0.022 cm^3 to 0.26 ± 0.037 cm^3) as compared to tumor control (group I). Moreover, the developed formulation (OL-FML) showed a significantly higher rate of tumor growth inhibition as compared to OL when administered in solution form ($p < 0.05$) (Fig. 13).

3.3.3. Change in body weight

After 30 days the maximum decrease in average body weight was observed in the case of the tumor control group (group I, −20.39 ± 3.429%). Initially, we have taken a total of 10 animals in each group but as the days passed some animals died in each group so we have taken into consideration the relative standard deviation in the presentation of data. OL-FML group (group III) was able to resist the negative change in body weight and showed a non-significant change as compared to normal control group. There were non-significant difference observed in OL treated group (group II) animals as compared to tumor control group (group I). Also, the effect of OL treated group (group II) was significantly lesser than group III ($p < 0.001$) (Fig. 12).

3.3.4. Kaplan–Meier (KM) survival analysis

KM survival plot for OL and OL-FML liposomes in comparison to normal and tumor control is presented in Fig. 11. The plot revealed that survival probability with OL-FML (group III) treatment was significantly higher as compared to the tumor control group (group I) ($p < 0.001$). However, OL treated group (group II) did not show statistically significant improvement in the survival probability with respect to tumor control group. Also, a significant and improved difference in survival probability was observed in OL-FML group with respect to the OL group ($p < 0.001$).

4. Discussion

OL loaded liposomal formulation was prepared by commonly used film hydration technique and further extruded to get nanosized vesicles with a narrow sized distribution. It is known that enhanced permeation and retention (EPR) effect play an important role in the passive targeting of cancer cells. Cancer cell membranes contain larger fenestrations (200 nm) as compared to normal cells which generally have 50 nm fenestrations. Thus, nanocarriers in size range of 50 to 200 nm are likely to be entrapped specifically within tumor tissues. Moreover, longer retention of the nanocarriers is also observed due to the feeble lymphatic system within the tumor site [21]. OL-FML developed was well within the desired particle size range. The particle size and the uniformity of articles were also evident forms the SEM and TEM microphotograph. Cancer cells have been proven to possess negatively charged surface due to lactic acid secretion in oxygen-deficient cells [22]. The positive zeta potential of the developed liposome (OL-FML) was obtained because of DC cholesterol incorporation within lipid bilayer as it has one positive charge head group. The positively charged liposomes were aimed to provide additional tumor retention. However, at this low positive potential, there is a chance of low electrostatic repulsion and decrease stability. But the presence of PEG on the liposome surface would have provided a strong inter-bilayer repulsion to

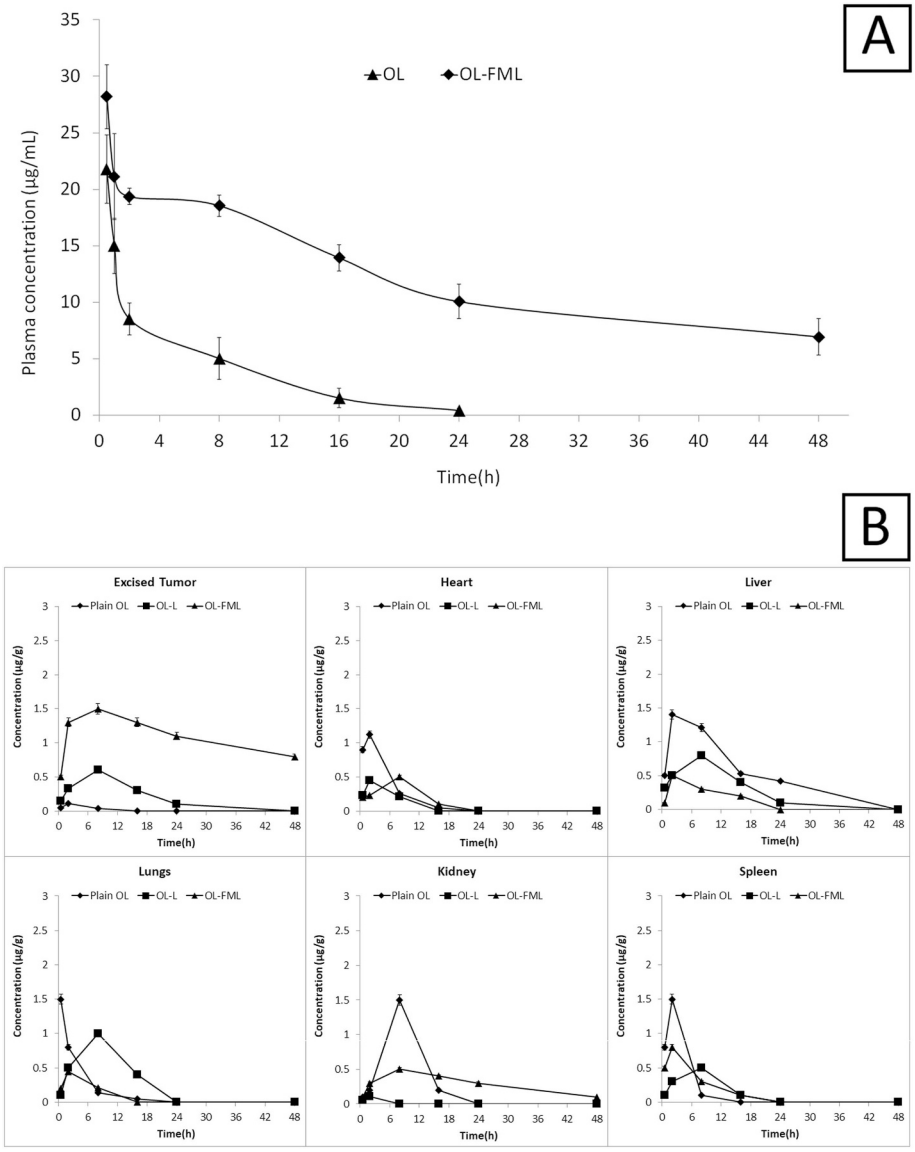

Fig. 10. A) Pharmacokinetic profile after the intravenous administration of OL and OL-FML. Longer and enhanced plasma concentration with OL-FML was achieved due to the stealth effect. B) Biodistribution study showing the concentration of OL at different time interval in various organs and tumor tissue.

Table 1
The pharmacokinetic parameters calculated after intravenous administration of OL and OL-FML (OL dose = 25 mg/Kg).

Parameters	OL	OL-FML
Intercept	1.23 ± 0.049	1.352 ± 0.011
Slope	−0.066 ± 0.013	−0.011 ± 0.001
K_{el} (h^{-1})	0.154 ± 0.031	0.026 ± 0.004
$t_{1/2}$ (h)	4.529 ± 0.904	26.068 ± 4.188
C_{max} (µg/mL)	21.774 ± 3.03	28.194 ± 2.826
T_{max} (h)	0.5	0.5
Cp_0 (µg/mL)	17.026 ± 1.904	22.51 ± 0.585
V_d (mL)	44.142 ± 5.096	33.32 ± 0.869
Cl (mL/h)	6.781 ± 1.041	0.888 ± 0.121
$AUC_{0\text{-}t}$ (µg·h/mL)	101.233 ± 16.584	379.256 ± 13.384
$AUC_{0\text{-}\infty}$ (µg·h/mL)	104.112 ± 18.374	641.779 ± 103.764

K_{el} (h^{-1}) = elimination rate constant; $t_{1/2}$ (h) = elimination half-life; C_{max} (µg/mL) = maximum plasma concentration; T_{max} (h) = time to reach C_{max}; Cp_0 (µg/mL) = concentration at zero time; V_d (mL) = volume of distribution; Cl (mL/h) = clearance; AUC = area under curve.

overcome the attractive Van der Waals forces and decreased aggregation [23]. Comparative differential scanning calorimetry (DSC) thermogram of OL and OL-FML showed a diminished peak of OL in the liposomes which suggest that OL molecules were majorly enclosed within the vesicular core. However, there is a possibility of some OL molecules to be adsorbed on the surface of liposomes because of the polar surface as well as a presence for hydrophilic PEG strands. This effect was evident from in vitro drug release profile where a burst release effect was observed in which 27.54 ± 2.995% of OL was released from OL-FML within 1 h of study. It was followed by a sustained release pattern continuing up to 24 h. OL solution showed a typical release pattern of any aqueous soluble drug. > 75% of OL was released within a 1st hour of study. Cell viability study is considered one of the preliminary study to determine the anticancer efficacy of the molecules and drug delivery system. Our observations showed significant inhibition of cell viability by OL-FML with respect to OL at all selected concentration. The concentration vs % cell viability plot was transformed to logarithmic plot to get straight line curves which were used to calculate the IC_{50}. The marked lowering of IC_{50} with OL-FML was seen as compared to OL solution. The multiple mechanisms can be attributed to this increased activity. The attraction of positively charged liposomes

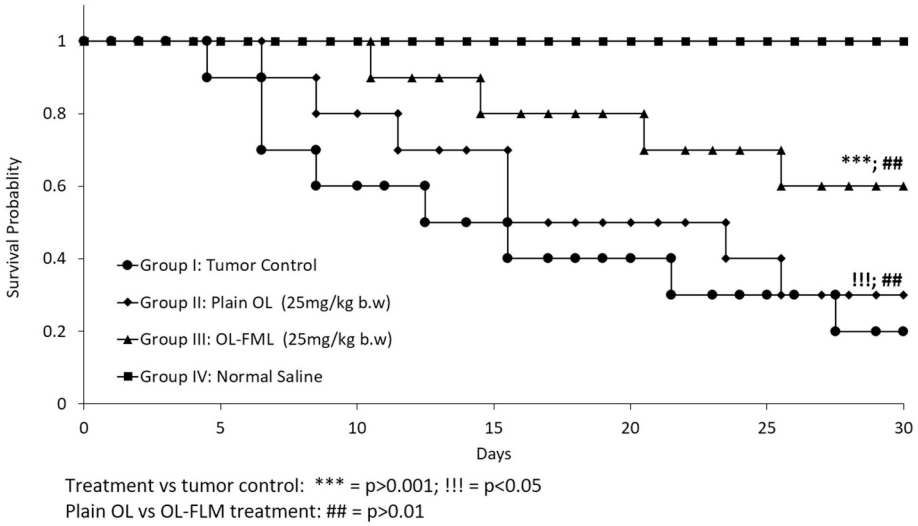

Fig. 11. Kaplan Meier survival plots for 30 days study. Tumor control (group I, Normal Saline, Tumor +ve), negative control (group IV, Normal Saline, Tumor -ve), OL treated (group II, 25 mg/kg OL, Tumor +ve), OL-FML treated (group III, 25 mg/kg OL, Tumor +ve).

towards negatively charged cell surface, anchoring of folate moiety to its receptor, cellular surface adsorption of liposomes and consequent endocytosis. These phenomena have been well explained in a previous report [24]. It has been shown that insistent oxidative stress within cancer cells activates growth-promoting signals and apoptosis [25]. OL possess excellent antioxidant and anti-inflammatory effects which can reduce inhibitory effects on apoptotic pathways [26]. Also, OL down regulates pAkt leading to inhibition of Akt signaling is also responsible for induction of apoptosis in cancer cells [27]. So, the apoptotic effects were expected to be more pronounced with increased cellular uptake of OL. The cell apoptosis assay confirmed the hypothesis as there was increased phosphatidylserine externalization (demarcated by increased Annexin V binding) in case of OL-FML treatment as compared to plain OL. During programmed cell death, there are alterations in the nuclear material which can be analyzed using TUNEL assay. OL has been evaluated for *in situ* TUNEL of nicked DNA in SH-SY5Y cell line and proven to show apoptosis [28]. Similarly, TUNEL assay has shown the pro-apoptotic effect of both OL and OL-FML in 22Rv1 cells. However, the effect was significantly enhanced with OL-FML. Another important apoptotic marker is a decrease in mitochondrial membrane potential ($\Delta\psi m$), which is indicative of early apoptotic transformation. The reduction of $\Delta\psi m$ after inner mitochondrial membrane permeabilization activates the release of numerous apoptotic factors. The decrease in mitochondrial membrane potential of olive leaf extract has been previously demonstrated by Bali et al. [29]. OL-FML has shown to enhance this effect in 22Rv1 cells as compared to OL. Caspase-3 activation is generally believed to be a hallmark of apoptosis. OL-FML treatment was able to activate caspase-3 at a significantly higher level as compared to OL. *In vivo* pharmacokinetic study revealed > 6 times increase in $AUC_{0-\infty}$ of OL when administered as OL-FML as compared to OL solution. Also, there was a reduced rate of elimination, increased elimination half-life and reduced clearance observed with OL-FML (Table 1). The major contributor of this result is polyethylene glycol (PEG) embedding within the lipid bilayer of the liposome. PEG was amalgamated on the liposomal surface by anchoring a cross-linked conjugated phospholipid (DSPE-mPEG2000) on the surface of the liposome. PEG imparts long circulating effect or stealth effect in liposomes by lowering reticuloendothelial system (RES) or mononuclear phagocyte system

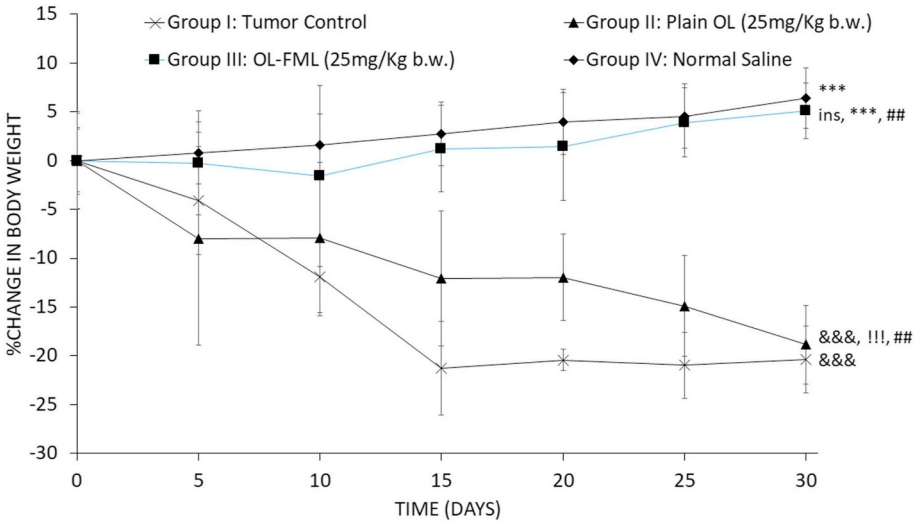

Fig. 12. Percentage change in body weight in different group of animals.

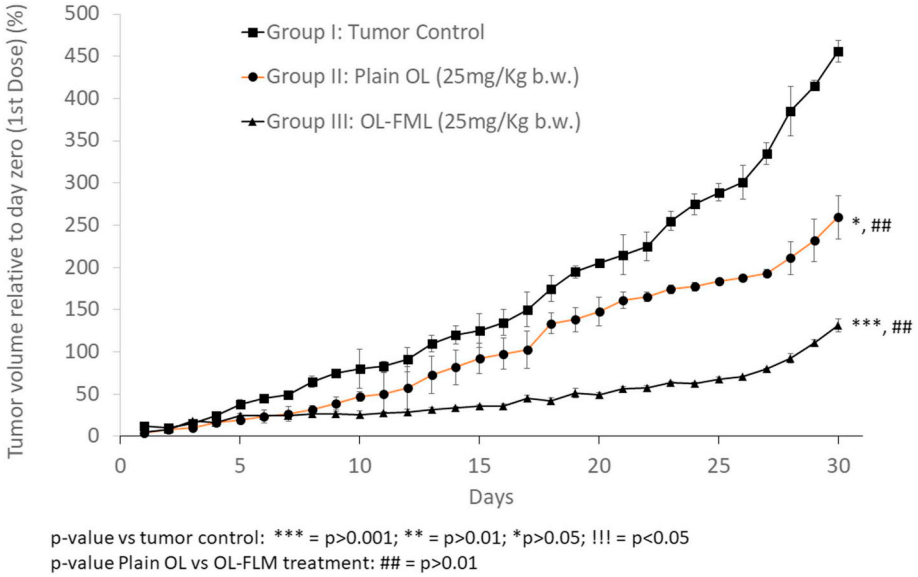

Fig. 13. Tumor growth inhibition study showing a significantly higher rate of inhibition by the developed formulation (OL-FML) of as compared to OL when administered in solution form.

(MPS) uptake [30]. Also, through OL-FML, oleuropein metabolism might be hindered and enhanced plasma concentration was achieved for the longer duration of time as compared to plain OL administration. The biodistribution study showed a well pronounced tumor targeting effect with OL-FML administration as compared to plain OL as well as OL-L (liposomes without folate moiety). There was a sustained maintenance of OL concentration in tumor tissue with OL-FML even after 48 h. OL-L also showed some increase in OL concentration during 8 h but declined gradually to a negligible amount in 48 h. This could be due to long circulation and EPR (enhanced permeation and retention effect) with OL-L. A significant higher retention of OL-FML might be due to active targeting by folate moiety as well as passive targeting (Stealth and EPR effect). In other organs, there was a quick and high increase and fast decline in concentration of OL when administered in plain form as compared to both OL-L and OL-FML. This might be due to higher volume of distribution (Table 1) with plain OL. With PEGylated liposomes (OL-L and OL-FML), the concentration was gradually increased and decreased but up to lesser extent with respect to plain OL, this is due to the long circulation and RES escape. This effect was directly translated into the *in vivo* pharmacodynamics in mice model. The goal of Kaplan Meier survival analysis was to estimate a population survival curve from a sample. If every subject is followed until death, the curve may be estimated simply by computing the fraction surviving at each time. However, in most clinical studies patients tend to drop out, become lost to follow up, move away, etc. (Censored data). A Kaplan-Meier analysis allows estimation of survival over time, even when patients drop out or are studied for different lengths of time (censored data). Many studies also used this method for animal survival analysis [31,32]. KM survival plot revealed remarkable improvement in survival probability after OL-FML treatment. The effect of plain OL administration did not show significant improvement as compared to control. The long circulation time, EPR effect, binding of liposomes to folate receptors and increased endocytosis are the factors responsible for such notable improvement in survival probability with OL-FML administration. Reduction in body weight is considered one of the most common symptoms appearing in nearly all types of cancers [33]. This effect was clearly manifested in tumor control (Tumor-induced + Normal saline) group animals as compared to normal control group. Anorexia, nutritional loss, tumor-host nutrient competition, nutrient uptake by tumors, increased energy expenditure are some of the main causes of weight loss. Our study showed a significant reduction in tumor volume by OL-FML treatment as compared to plain OL treatment. This effect was directly reflected in body weight profile.

5. Conclusion

The effect of oleuropein (OL) loaded surface functionalized folate – PEG liposomes (OL-FML) to inhibit the 22Rv1 prostate cancer cells was studied and compared with plain oleuropein solution. Cell viability assay and various apoptosis studies including phosphatidylserine externalization assay, TUNEL assay, analysis of mitochondrial membrane potential and caspase-3 activation assay were performed. In vivo pharmacokinetic study revealed that OL-FML was able to maintain a longer and increased the concentration of oleuropein in blood. Finally, the comparative effect of the developed system and plain oleuropein was studied in tumor-induced mice model in terms of change in tumor volume, body weight, and the survival probability. In each study, a noticeable improvement in the induced condition was observed with OL-FML treatment. The effects were majorly attributed to passive targeting mechanisms including long circulation, EPR, and liposomal endocytosis as well as active targeting through overexpressed folate receptor binding.

Acknowledgment

This article was funded by the ICSR, Umm Al-Qura University, Makkah, Saudi Arabia (Grant no. 43509010). We would like to acknowledge Dr. Wael M. AlSalim for laboratory work and assistance in writing the manuscript. We are also thankful to the department secretary Mohammed Iezaz Safar Ali for his secretarial and clerical support.

Conflict of interest

The authors declare that they have no competing interests.

References

[1] C. Global Burden of Disease Cancer, C. Fitzmaurice, C. Allen, R.M. Barber, L. Barregard, Z.A. Bhutta, H. Brenner, D.J. Dicker, O. Chimed-Orchir, R. Dandona, L. Dandona, T. Fleming, M.H. Forouzanfar, J. Hancock, R.J. Hay, R. Hunter-Merrill, C. Huynh, H.D. Hosgood, C.O. Johnson, J.B. Jonas, J. Khubchandani, G.A. Kumar, M. Kutz, Q. Lan, H.J. Larson, X. Liang, S.S. Lim, A.D. Lopez, M.F. MacIntyre, L. Marczak, N. Marquez, A.H. Mokdad, C. Pinho, F. Pourmalek, J.A. Salomon, J.R. Sanabria, L. Sandar, B. Sartorius, S.M. Schwartz, K.A. Shackelford, K. Shibuya,

J. Stanaway, C. Steiner, J. Sun, K. Takahashi, S.E. Vollset, T. Vos, J.A. Wagner, H. Wang, R. Westerman, H. Zeeb, L. Zoeckler, F. Abd-Allah, M.B. Ahmed, S. Alabed, N.K. Alam, S.F. Aldhahri, G. Alem, M.A. Alemayohu, R. Ali, R. Al-Raddadi, A. Amare, Y. Amoako, A. Artaman, H. Asayesh, N. Atnafu, A. Awasthi, H.B. Saleem, A. Barac, N. Bedi, I. Bensenor, A. Berhane, E. Bernabe, B. Betsu, A. Binagwaho, D. Boneya, I. Campos-Nonato, C. Castaneda-Orjuela, F. Catala-Lopez, P. Chiang, C. Chibueze, A. Chitheer, J.Y. Choi, B. Cowie, S. Damtew, J. das Neves, S. Dey, S. Dharmaratne, P. Dhillon, E. Ding, T. Driscoll, D. Ekwueme, A.Y. Endries, M. Farvid, F. Farzadfar, J. Fernandes, F. Fischer, G.H. TT, A. Gebru, S. Gopalani, A. Hailu, M. Horino, N. Horita, A. Husseini, I. Huybrechts, M. Inoue, F. Islami, M. Jakovljevic, S. James, M. Javanbakht, S.H. Jee, A. Kasaeian, M.S. Kedir, Y.S. Khader, Y.H. Khang, D. Kim, J. Leigh, S. Linn, R. Lunevicius, H.M.A. El Razek, R. Malekzadeh, D.C. Malta, W. Marcenes, D. Markos, Y.A. Melaku, K.G. Meles, W. Mendoza, D.T. Mengiste, T.J. Meretoja, T.R. Miller, K.A. Mohammad, A. Mohammadi, S. Mohammed, M. Moradi-Lakeh, G. Nagel, D. Nand, Q. Le Nguyen, S. Nolte, F.A. Ogbo, K.E. Oladimeji, E. Oren, M. Pa, E.K. Park, D.M. Pereira, D. Plass, M. Qorbani, A. Radfar, A. Rafay, M. Rahman, S.M. Rana, K. Soreide, M. Satpathy, M. Sawhney, S.G. Sepanlou, M.A. Shaikh, J. She, I. Shiue, H.R. Shore, M.G. Shrime, S. So, S. Soneji, V. Stathopoulou, K. Stroumpoulis, M.B. Sufiyan, B.L. Sykes, R. Tabares-Seisdedos, F. Tadese, B.A. Tedla, G.A. Tessema, J.S. Thakur, B.X. Tran, K.N. Ukwaja, B.S.C. Uzochukwu, V.V. Vlassov, E. Weiderpass, M. Wubshet Terefe, H.G. Yebyo, H.H. Yimam, N. Yonemoto, M.Z. Younis, C. Yu, Z. Zaidi, M.E.S. Zaki, Z.M. Zenebe, C.J.L. Murray, M. Naghavi, Global, regional, and national cancer incidence, mortality, years of life lost, years lived with disability, and disability-adjusted life-years for 32 cancer groups, 1990 to 2015: a systematic analysis for the Global Burden of Disease Study, JAMA Oncol. 3 (4) (2017) 524–548.

[2] N.J. Clegg, J. Wongvipat, J.D. Joseph, C. Tran, S. Ouk, A. Dilhas, Y. Chen, K. Grillot, E.D. Bischoff, L. Cai, A. Aparicio, S. Dorow, V. Arora, G. Shao, J. Qian, H. Zhao, G. Yang, C. Cao, J. Sensintaffar, T. Wasielewska, M.R. Herbert, C. Bonnefous, B. Darimont, H.I. Scher, P. Smith-Jones, M. Klang, N.D. Smith, E. De Stanchina, N. Wu, O. Ouerfelli, P.J. Rix, R.A. Heyman, M.E. Jung, C.L. Sawyers, J.H. Hager, ARN-509: a novel antiandrogen for prostate cancer treatment, Cancer Res. 72 (6) (2012) 1494–1503.

[3] O. Benavente-Garcıa, J. Castillo, J. Lorente, A. Ortuno, J. Del Rio, Antioxidant activity of phenolics extracted from Olea europaea L. leaves, Food Chem. 68 (4) (2000) 457–462.

[4] F. Visioli, A. Poli, C. Gall, Antioxidant and other biological activities of phenols from olives and olive oil, Med. Res. Rev. 22 (1) (2002) 65–75.

[5] J. Han, T.P. Talorete, P. Yamada, H. Isoda, Anti-proliferative and apoptotic effects of oleuropein and hydroxytyrosol on human breast cancer MCF-7 cells, Cytotechnology 59 (1) (2009) 45–53.

[6] R. Acquaviva, C. Di Giacomo, V. Sorrenti, F. Galvano, R. Santangelo, V. Cardile, S. Gangia, N. D'Orazio, N.G. Abraham, L. Vanella, Antiproliferative effect of oleuropein in prostate cell lines, Int. J. Oncol. 41 (1) (2012) 31–38.

[7] M. Carrera-González, M. Ramírez-Expósito, M. Mayas, J. Martínez-Martos, Protective role of oleuropein and its metabolite hydroxytyrosol on cancer, Trends Food Sci. Technol. 31 (2) (2013) 92–99.

[8] P. Del Boccio, A. Di Deo, A. De Curtis, N. Celli, L. Iacoviello, D. Rotilio, Liquid chromatography–tandem mass spectrometry analysis of oleuropein and its metabolite hydroxytyrosol in rat plasma and urine after oral administration, J. Chromatogr. B 785 (1) (2003) 47–56.

[9] S. Kano, H. Komada, L. Yonekura, A. Sato, H. Nishiwaki, H. Tamura, Absorption, metabolism, and excretion by freely moving rats of 3,4-DHPEA-EDA and related polyphenols from olive fruits (Olea europaea), J. Nutr. Metab. 2016 (2016) 10.

[10] M. Bock, E.B. Thorstensen, J.G. Derraik, H.V. Henderson, P.L. Hofman, W.S. Cutfield, Human absorption and metabolism of oleuropein and hydroxytyrosol ingested as olive (Olea europaea L.) leaf extract, Mol. Nutr. Food Res. 57 (11) (2013) 2079–2085.

[11] I. Ahmad, S. Akhter, M. Anwar, S. Zafar, R.K. Sharma, A. Ali, F.J. Ahmad, Supercritical anti-solvent technique assisted synthesis of thymoquinone liposomes for radioprotection: formulation optimization, in-vitro and in-vivo studies, Int. J. Pharm. 523 (1) (2017) 398–409.

[12] A. Singh, I. Ahmad, S. Akhter, M. Zaki Ahmad, Z. Iqbal, F.J. Ahmad, Thymoquinone: major molecular targets, prominent pharmacological actions and drug delivery concerns, Curr. Bioact. Compd. 8 (4) (2012) 334–344.

[13] A. Gabizon, F. Martin, Polyethylene glycol-coated (pegylated) liposomal doxorubicin, Drugs 54 (4) (1997) 15–21.

[14] M. Riaz, M. Riaz, X. Zhang, C. Lin, K. Wong, X. Chen, G. Zhang, A. Lu, Z. Yang, Surface functionalization and targeting strategies of liposomes in solid tumor therapy: a review, Int. J. Mol. Sci. 19 (1) (2018) 195.

[15] B. Xiang, D.W. Dong, N.Q. Shi, W. Gao, Z.Z. Yang, Y. Cui, D.Y. Cao, X.R. Qi, PSA-responsive and PSMA-mediated multifunctional liposomes for targeted therapy of prostate cancer, Biomaterials 34 (28) (2013) 6976–6991.

[16] C. Grizis, J. Atta-Politou, M.A. Koupparis, Simultaneous determination of oleuropein and tyrosol in plasma using high performance liquid chromatography with UV detection, J. Liq. Chromatogr. Relat. Technol. 26 (4) (2003) 599–616.

[17] A.M. Nassir, N. Shahzad, I.A.A. Ibrahim, I. Ahmad, S. Md, M.R. Ain, Resveratrol-loaded PLGA nanoparticles mediated programmed cell death in prostate cancer cells, Saudi Pharm. J. 26 (6) (2018) 876–885.

[18] S. Sheth, S. Jajoo, T. Kaur, D. Mukherjea, K. Sheehan, L.P. Rybak, V. Ramkumar, Resveratrol reduces prostate cancer growth and metastasis by inhibiting the Akt/microRNA-21 pathway, PLoS One 7 (12) (2012) e51655.

[19] Q. Chen, S. Ganapathy, K.P. Singh, S. Shankar, R.K. Srivastava, Resveratrol induces growth arrest and apoptosis through activation of FOXO transcription factors in prostate cancer cells, PLoS One 5 (12) (2010) e15288.

[20] A.N. Lukyanov, V.P. Torchilin, Autoclaving of liposomes, J. Microencapsul. 11 (6) (1994) 669–672.

[21] A. Rodzinski, R. Guduru, P. Liang, A. Hadjikhani, T. Stewart, E. Stimphil, C. Runowicz, R. Cote, N. Altman, R. Datar, S. Khizroev, Targeted and controlled anticancer drug delivery and release with magnetoelectric nanoparticles, Sci. Rep. 6 (2016) 20867.

[22] B. Chen, W. Le, Y. Wang, Z. Li, D. Wang, L. Ren, L. Lin, S. Cui, J.J. Hu, Y. Hu, P. Yang, R.C. Ewing, D. Shi, Z. Cui, Targeting negative surface charges of Cancer cells by multifunctional nanoprobes, Theranostics 6 (11) (2016) 1887–1898.

[23] D. Needham, T.J. McIntosh, D.D. Lasic, Repulsive interactions and mechanical stability of polymer-grafted lipid membranes, Biochim. Biophys. Acta 1108 (1) (1992) 40–48.

[24] C.R. Miller, B. Bondurant, S.D. McLean, K.A. McGovern, D.F. O'Brien, Liposome–cell interactions in vitro: effect of liposome surface charge on the binding and endocytosis of conventional and sterically stabilized liposomes, Biochemistry 37 (37) (1998) 12875–12883.

[25] N.S. Brown, R. Bicknell, Hypoxia and oxidative stress in breast cancer: oxidative stress: its effects on the growth, metastatic potential and response to therapy of breast cancer, Breast Cancer Res. 3 (5) (2001) 323–327.

[26] I. Hassen, H. Casabianca, K. Hosni, Biological activities of the natural antioxidant oleuropein: exceeding the expectation – a mini-review, J. Funct. Foods 18 (2015) 926–940.

[27] F.Y. Tang, C.J. Shih, L.H. Cheng, H.J. Ho, H.J. Chen, Lycopene inhibits growth of human colon cancer cells via suppression of the Akt signaling pathway, Mol. Nutr. Food Res. 52 (6) (2008) 646–654.

[28] M. Secme, C. Eroglu, Y. Dodurga, G. Bagci, Investigation of anticancer mechanism of oleuropein via cell cycle and apoptotic pathways in SH-SY5Y neuroblastoma cells, Gene 585 (1) (2016) 93–99.

[29] E.B. Bali, V. Ergin, L. Rackova, O. Bayraktar, N. Küçükboyacı, Ç. Karasu, Olive Leaf Extracts Protect Cardiomyocytes against 4-Hydroxynonenal-induced Toxicity In Vitro: Comparison with Oleuropein, Hydroxytyrosol, and Quercetin, (2014).

[30] M.L. Immordino, F. Dosio, L. Cattel, Stealth liposomes: review of the basic science, rationale, and clinical applications, existing and potential, Int. J. Nanomedicine 1 (3) (2006) 297–315.

[31] D. Zhang, E.-M.E. Hedlund, S. Lim, F. Chen, Y. Zhang, B. Sun, Y. Cao, Antiangiogenic agents significantly improve survival in tumor-bearing mice by increasing tolerance to chemotherapy-induced toxicity, Proc. Natl. Acad. Sci. 108 (10) (2011) 4117–4122.

[32] M. Vermulst, J.H. Bielas, G.C. Kujoth, W.C. Ladiges, P.S. Rabinovitch, T.A. Prolla, L.A. Loeb, Mitochondrial point mutations do not limit the natural lifespan of mice, Nat. Genet. 39 (4) (2007) 540–543.

[33] A. Theologides, Weight loss in cancer patients, CA Cancer J. Clin. 27 (4) (1977) 205–208.